Self-consistent Hartree-Fock based random phase approximation and the spurious state mixing

B. K. Agrawal,[1] S. Shlomo,[1] and A. I. Sanzhur[1,2]
[1]*Cyclotron Institute, Texas A&M University, College Station, Texas 77843*
[2]*Institute for Nuclear Research, Kiev 03680, Ukraine*
(Received 25 October 2002; published 25 March 2003)

We use a fully self-consistent Hartree-Fock (HF) based continuum random phase approximation (CRPA) to calculate strength functions $S(E)$ and transition densities $\rho_t(r)$ for isoscalar giant resonances with multipolarities $L=0$, 1, and 2 in ^{80}Zr nucleus. In particular, we consider the effects of spurious state mixing (SSM) in the isoscalar giant dipole resonance and extend the projection method to determine the mixing amplitude of the spurious state so that properly normalized $S(E)$ and $\rho_t(r)$, having no contribution due to SSM, can be obtained. For the calculation to be highly accurate, we use a very fine radial mesh (0.04 fm) and zero smearing width in HF-CRPA calculations. We use our most accurate results as a basis to (i) establish the credibility of the projection method, employed to eliminate the SSM, and (ii) to assess the consequences of the common violations of self-consistency, often encountered in actual implementation of HF based CRPA and discretized RPA (DRPA) published in the literature, on the values of $S(E)$ and $\rho_t(r)$. This is achieved by varying the radial mesh size, the particle-hole interaction, the smearing parameter, and the particle-hole energy cutoff used in the HF-RPA calculations.

DOI: 10.1103/PhysRevC.67.034314 PACS number(s): 21.60.Jz, 24.30.Cz, 21.65.+f

I. INTRODUCTION

The Hartree-Fock (HF) based random phase approximation (RPA) has been a very successful theory in providing microscopic description of phenomena associated with collective motion in nuclei [1]. Accurate information for important physical quantities can be obtained by comparing the experimentally deduced strength function distribution $S(E)$ with the results obtained from HF-RPA theory. In particular, the strength function distributions of the isoscalar giant monopole resonance (ISGMR) and the isoscalar giant dipole resonance (ISGDR) are quite sensitive to the value of the nuclear matter incompressibility coefficient K_{nm} [1–4], a very important physical quantity since it is directly related to the curvature of the nuclear matter equation of state.

Over the past two decades, a significant amount of experimental work has been carried out to identify the strength distributions of the isoscalar giant resonances in nuclei, particularly the ISGMR [3] and ISGDR [5]. The main development in the area of experimental investigation of the isoscalar giant resonances is the high accuracy data of excitation cross section by α-particle scattering, obtained at Texas A&M University using a beam analysis system, a multipole-dipole-multipole spectrometer, and a broad range multiwire proportional counter. This led to the discovery of a high-lying structure in the strength function of the ISGMR and the location of the ISGMR in light nuclei. Furthermore, accurate data on the ISGDR has been obtained for a wide range of nuclei [5]. This has led to renewed interest in the nuclear response function and the need to carry out detailed and accurate calculations of $S(E)$ and the transition density ρ_t within the HF-RPA theory. In particular, there have been quite a few recent nonrelativistic HF-RPA [6–10] and relativistic mean-field based RPA [11,12] calculations of the ISGDR, considering the issues of (i) spurious state mixing (SSM), (ii) the strength of the lower component (at $1\hbar\omega$), and (iii) the value of K_{nm} deduced from the centroid energy E_1 of the ISGDR compression mode (at $3\hbar\omega$).

Comparison between the recent data on the ISGMR and the results of HF based RPA calculations confirms the value of $K_{nm}=210\pm 20$ MeV, determined earlier in Ref. [4]. It was first pointed out in Ref. [13] that the HF-RPA results for E_1, obtained with interactions adjusted to reproduce the ISGMR data, are higher than the experimental values [14,15] by more than 3 MeV and thus this discrepancy between theory and experiment raises doubts concerning the unambiguous extraction of K_{nm} from centroid energies of compression modes. This discrepancy between theory and experiment was also reported in more recent experiments [5,16]. Recently, Shlomo and Sanzhur [9] have resolved this discrepancy by carrying out accurate microscopic calculations for $S(E)$ and the excitation cross section $\sigma(E)$ of the ISGDR, within the folding model distorted-wave Born approximation, with ρ_t obtained from HF-RPA calculations and corrected for the SSM. They demonstrated that the calculated $\sigma(E)$ drops below the experimental sensitivity in the region of high excitation energy containing 30–40 % of the ISGDR energy weighted sum rule (EWSR). This missing strength leads to a reduction of more than 3.0 MeV in the value of E_1 and thus explains the discrepancy between theory and experiment.

Clearly, accurate calculations of $S(E)$ and $\sigma(E)$ are needed. In fully self-consistent HF-RPA calculations, the spurious isoscalar dipole ($T=0$, $L=1$) state (associated with the center of mass motion) appears at energy $E=0$ and no SSM in the ISGDR occurs. It was pointed out in Ref. [9] that none of the results for $S(E)$ and ρ_t published in the literature were obtained in fully self-consistent calculations. In some RPA calculations, the mean field and the particle-hole interaction V_{ph} are chosen independently. Although this approach can provide physical insight into the structure of giant resonances, it cannot be used to accurately determine important physical quantities such as K_{nm}. In a self-consistent HF-RPA calculation [17], one starts by adopting a specific effective

nucleon-nucleon interaction, V_{12}, such as the Skyrme interaction, and carries out HF calculations. The parameters of the interaction are determined by a fit to properties of nuclei (binding energies, radii, etc.). Then, one solves the RPA equation using the particle-hole (p-h) interaction V_{ph} which is consistent with V_{12}. However, though not always stated in the literature, self-consistency is violated in actual implementations of the nonrelativistic RPA (and relativistic RPA) calculations. One usually makes the following approximations: (i) using a V_{ph} which is not consistent with V_{12} by commonly neglecting the two-body Coulomb and spin-orbit interactions in V_{ph} and approximating the momentum dependent parts in V_{ph}, (ii) limiting the p-h space in a discretized calculation by a cutoff energy E_{ph}^{max}, and (iii) introducing a smearing parameter (i.e., a Lorentzian with $\Gamma/2$). The consequences of these violations of self-consistency and of numerical inaccuracy on $S(E)$ and ρ_t are usually ignored in the literature.

In this work, we present results of detailed investigations of the consequences of common violations of self-consistency in actual implementations of HF based RPA for determining the response functions $S(E)$ and ρ_t of isoscalar multipole ($L=0,1$, and 2) giant resonances. In particular, we consider the ISGDR and concentrate on the effects of the SSM. We determine the effects of a violation of self-consistency by comparing the calculated results for $S(E)$ and ρ_t with those obtained from highly accurate fully self-consistent HF– continuum RPA (HF-CRPA) calculations [18]. We also extend the projection method for eliminating the effects of SSM, described in Ref. [9], to properly normalize $S(E)$ and ρ_t and determine the mixing amplitude of the spurious state in the ISGDR.

For completeness and presentation of our results, we provide in Sec. II the basic expressions used in the calculations. We also present an extension of Green's function based derivation of the projection operator method for eliminating the effects of the SSM, described in Ref. [9], to account for the proper normalization of the $S(E)$ and $\rho_t(\mathbf{r})$ of the ISGDR and determine the mixing amplitude of the spurious state obtained in HF-RPA calculations. We emphasize here that the method is quite general and applicable for any scattering operator F and for any numerical method used in carrying out the RPA calculation, such as configuration space RPA, coordinate space (continuum and discretized) RPA, and with and without the addition of smearing.

In Sec. III, we present and discuss our results. We first present the results of a highly accurate and fully self-consistent HF-CRPA calculation of $S(E)$ and $\rho_t(r)$ in ^{80}Zr, which we use as a basis for a comparison with results obtained with common violations of self-consistency. These accurate fully self-consistent HF-CRPA results were obtained using $\Gamma=0$ (i.e., no smearing) and very small mesh sizes of $dr_{HF}=0.04$ fm and $dr_{RPA}=0.04$ fm with corresponding numbers of mesh points $N_{HF}=900$ and $N_{RPA}=300$ used in the HF and the CRPA calculations, respectively. We note that the values of $S(E)$ and $\rho_t(r)$ associated with a bound RPA state were deduced from the residue of the RPA Green's function. Next, we present our results of fully self-consistent HF-CRPA calculations (with $\Gamma=0$) carried out using various mesh sizes dr_{HF} and dr_{RPA} and discuss the issue of numerical accuracy. We then present the results obtained with certain violations of self-consistency in CRPA and discretized RPA (DRPA) calculations and compare these results with the highly accurate fully self-consistent results over the whole range of excitation energies. We would like to point out that comparing the total energy weighted transition strength (EWTS) with the EWSR may lead to incorrect conclusions. We emphasize that in the present work, we establish the accuracy of the projection operator method and provide assessments of the effects of common violations of self-consistency, often encountered in actual implementations of HF-RPA published in the literature, on the $S(E)$, E_L, and ρ_t of the isoscalar giant resonances with $L=0$, 1, and 2. Preliminary results of the present work were presented earlier [19]. We note that very recently the accuracy of the projection operator method in eliminating the effects of the SSM on $S(E)$ and ρ_t of the ISGDR was investigated in Refs. [9,20]. However, in these works, the calculations, carried out using a mesh size $dr \geqslant 0.1$ fm, were not fully self-consistent and thus it is not possible to determine the consequences of the violations of self-consistency on $S(E)$ and ρ_t. Moreover, the applicability of the projection operator was only inferred by comparing the total EWTS with the EWSR. In Sec. IV, we state our conclusions.

II. FORMALISM

In the following, we provide for completeness and presentation of our results, the basic expressions used in the calculations. Furthermore, we extend Green's function based derivation of the projection operator method [9] for eliminating the effects of the SSM to also obtain properly normalized $S(E)$ and $\rho_t(\mathbf{r})$ of the ISGDR and determine the mixing amplitude of the spurious state.

The RPA Green's function G [17,18] is given by

$$G = G_0(1+V_{ph}G_0)^{-1}, \tag{1}$$

where G_0 is the free p-h Green's function given by

$$G_0(\mathbf{r},\mathbf{r}',\omega) = -\sum_h \phi_h(\mathbf{r})\left[\frac{1}{H_0-\epsilon_h-\omega} + \frac{1}{H_0-\epsilon_h+\omega}\right]\phi_h(\mathbf{r}'). \tag{2}$$

Here, H_0 is the HF Hamiltonian and ϵ_h and ϕ_h are the single-particle energy and the wave function of the occupied state, respectively. The continuum effects (particle escape width) are included by using

$$G_{lj}(\mathbf{r},\mathbf{r}',E) = \frac{1}{H_0-E} = -\frac{2m}{\hbar^2}u_{lj}(r_<)v_{lj}(r_>)/w, \tag{3}$$

where $r_<$ and $r_>$ are the the lesser and the greater of r and r', respectively, u and v are the regular and irregular solution of H_0, with the appropriate boundary conditions, respec-

tively, and w is the Wronskian. The strength function $S(E)$ and transition density ρ_t associated with the scattering operator

$$F=\sum_{i=1}^{A} f(\boldsymbol{r}_i) \tag{4}$$

are given by

$$S(E)=\sum_n |\langle 0|F|n\rangle|^2 \delta(E-E_n)=\frac{1}{\pi}\mathrm{Im}[\mathrm{Tr}(fGf)], \tag{5}$$

$$\rho_t(\boldsymbol{r},E)=\frac{\Delta E}{\sqrt{S(E)\Delta E}}\int f(\boldsymbol{r}')\left[\frac{1}{\pi}\mathrm{Im}G(\boldsymbol{r}',\boldsymbol{r},E)\right]d\boldsymbol{r}'. \tag{6}$$

Note that $\rho_t(\boldsymbol{r},E)$, as defined in Eq. (6), is associated with the transition strength in the region of $E\pm\Delta E/2$ and is consistent with

$$S(E)=\left|\int \rho_t(\boldsymbol{r},E)f(\boldsymbol{r})d\boldsymbol{r}\right|^2 \Big/ \Delta E. \tag{7}$$

It is important to note that $S(E)$ and ρ_t of a state at energy E_n below the particle escape threshold (or having a very small width) can be obtained from Eqs. (5) and (6), respectively, by replacing $(1/\pi)\mathrm{Im}G(\boldsymbol{r}',\boldsymbol{r},E)$ with

$$\lim_{E\to E_n} \mathrm{Re}G(\boldsymbol{r}',\boldsymbol{r},E)(E_n-E). \tag{8}$$

The energy weighted sum rule (EWSR) associated with the operator $f_{LM}=f(r)Y_{LM}$ is given by [1]

$$\mathrm{EWSR}(fY_{LM})=\int ES_{LM}(E)dE = \frac{\hbar^2}{2m}\frac{A}{4\pi}\left[\langle 0|\left(\frac{df}{dr}\right)^2+L(L+1)\left(\frac{f}{r}\right)^2|0\rangle\right]. \tag{9}$$

Using the equation of continuity and assuming that there is only one collective state [21,22] with energy E_{coll}, exhausting 100% of the EWSR associated with the scattering operator $f_{LM}=f(r)Y_{LM}$, one obtains the form for the corresponding transition density

$$\rho_t^{coll}(r)=-\frac{\hbar^2}{2m}\sqrt{\frac{2L+1}{\mathrm{EWSR}(f_{LM})E_{coll}}}\left[\left(\frac{1}{r}\frac{d^2}{dr^2}(rf)-\frac{L(L+1)}{r^2}f\right)\rho_0+\frac{df}{dr}\frac{d\rho_0}{dr}\right]. \tag{10}$$

Let us consider the scattering operators, Eq. (4), with

$$f(\boldsymbol{r})=f(r)Y_{1M}(\Omega), \quad f_1(\boldsymbol{r})=rY_{1M}(\Omega), \tag{11}$$

and write $(1/\pi)\mathrm{Im}G$ as the sum of separable terms

$$R(\boldsymbol{r}',\boldsymbol{r},E)=\frac{1}{\pi}\mathrm{Im}G(\boldsymbol{r}',\boldsymbol{r},E)=\sum_n d_n(E)\rho_n(\boldsymbol{r})\rho_n(\boldsymbol{r}'). \tag{12}$$

Note that $d_n(E)$ accounts for the energy dependence of $R(\boldsymbol{r}',\boldsymbol{r},E)$. In the case of a well-defined resonance, or in a discretized continuum calculation, the sum in Eq. (12) has only one term. In this case, ρ_n is proportional to the transition density associated with the resonance and may contain a spurious state contribution. In general, due to the smearing with $\Gamma/2$, the sum in Eq. (12) may contain quite a few terms. We now write ρ_n as

$$\rho_n(\boldsymbol{r})=a_n\rho_{n3}(\boldsymbol{r})+b_n\rho_{n1}(\boldsymbol{r}), \tag{13}$$

with

$$a_n^2+b_n^2=1.0, \tag{14}$$

where a_n and b_n are the amplitudes of the intrinsic state and the spurious state, respectively. Note that ρ_{n3}, associated with the ISGDR, fulfills the center of mass condition (for all n)

$$\langle f_1\rho_{n3}\rangle=\int f_1(\boldsymbol{r})\rho_{n3}(\boldsymbol{r})d\boldsymbol{r}=0. \tag{15}$$

We point out that in the projection method for eliminating the effects of SSM described in Ref. [9], it was assumed that $a_n=1.0$ [in Eq. (13)].

Following the derivation described in Ref. [9], we first note that all ρ_{n1} coincide with the coherent spurious state transition density $\rho_{ss}(\boldsymbol{r})$ [23],

$$\rho_{n1}(\boldsymbol{r})=\rho_{ss}(\boldsymbol{r})=-\sqrt{\frac{\hbar^2}{2m}\frac{4\pi}{AE_{ss}}}\frac{\partial\rho_0}{\partial r}Y_{1M}(\Omega), \tag{16}$$

where E_{ss} is the spurious state energy and ρ_0 is the ground state density of the nucleus. Note that ρ_{ss} in Eq. (16) is normalized to 100% of the energy weighted sum rule [see Eqs. (9) and (10)],

$$\mathrm{EWSR}(rY_{1M})=\frac{\hbar^2}{2m}\frac{3}{4\pi}A. \tag{17}$$

Looking for a projection operator that projects out $\rho_{n1}(\boldsymbol{r})$,

$$F_\eta=\sum_{i=1}^{A} f_\eta(\boldsymbol{r}_i)=F-\eta F_1, \tag{18}$$

with $f_\eta=f-\eta f_1$, we find that the value of η associated with ρ_{ss} is given by

$$\eta=\langle f\rho_{ss}\rangle/\langle f_1\rho_{ss}\rangle. \tag{19}$$

Using Eqs. (15) and (19), we have

$$S_\eta(E)=\langle f_\eta R f_\eta\rangle=\langle fR_{33}f\rangle, \tag{20}$$

where

$$R_{33}=\sum d_n(E)a_n^2\rho_{n3}(\boldsymbol{r})\rho_{n3}(\boldsymbol{r}'). \tag{21}$$

To determine ρ_t for the ISGDR, we first use Eqs. (6), (12), (13), (15), and (19) with F_η and obtain

$$\rho_\eta(\boldsymbol{r})=\frac{\Delta E}{\sqrt{S_\eta(E)\Delta E}}\sum c_n a_n[a_n\rho_{a3}(\boldsymbol{r})+b_n\rho_{ss}(\boldsymbol{r})], \tag{22}$$

with $c_n=d_n(E)\langle f_\eta\rho_{n3}\rangle$. To project out the spurious term from Eq. (22), we make use of Eq. (15) and obtain

$$\rho_t(\boldsymbol{r})=\rho_\eta(\boldsymbol{r})-b\rho_{ss}, \quad b=\langle f_1\rho_\eta\rangle/\langle f_1\rho_{ss}\rangle. \tag{23}$$

To properly normalize $S_\eta(E)$ and ρ_t, we have to determine the mixing amplitudes b_n of the spurious state in the ISGDR. These amplitudes can be obtained from the response function to the scattering operator f_1. Using Eqs. (13), (15), and (16) we obtained from Eq. (12)

$$S_1(E)=\langle f_1Rf_1\rangle=\langle f_1R_{11}f_1\rangle=\sum d_n(E)b_n^2\langle f_1\rho_{ss}\rangle^2. \tag{24}$$

Note that $\langle f_1\rho_{ss}\rangle$ can be obtained from the EWSR, Eq. (17),

$$\langle f_1\rho_{ss}\rangle^2=\frac{\hbar^2}{2m}\frac{3}{4\pi}A/E_{ss}, \tag{25}$$

and the SSM probabilities from

$$b_n^2=\frac{S_1(E_n)}{\langle f_1\rho_{ss}\rangle^2}. \tag{26}$$

In the present work, we limit our discussion to the operator $F_3=\Sigma_{i=1}^{A}f_3(\boldsymbol{r}_i)$, where $f(\boldsymbol{r})=f_3(\boldsymbol{r})=r^3Y_{1M}(\Omega)$. For this operator, the value of η associated with the spurious transition density (16) is

$$\eta=\frac{5}{3}\langle r^2\rangle, \tag{27}$$

and

$$S_\eta(E)=S_3(E)-2\eta S_{13}(E)+\eta^2S_1(E), \tag{28}$$

where $S_3(E)=\langle f_3Rf_3\rangle$ is the strength function associated with f_3 and $S_{13}=\langle f_1Rf_3\rangle$ is the nondiagonal strength function.

III. RESULTS AND DISCUSSIONS

In the following, we present our results for isoscalar giant resonances ($L=0$, 1, and 2) obtained within the HF based RPA framework as briefly outlined in the preceding section. Calculations are performed for ^{80}Zr ($N=Z=40$), as an example. The two-body interaction V_{12} is taken to be of a simplified Skyrme type,

$$V_{12}=\delta(\boldsymbol{r}_1-\boldsymbol{r}_2)\left[t_0+\frac{1}{6}t_3\rho^\alpha\left(\frac{\boldsymbol{r}_1+\boldsymbol{r}_2}{2}\right)\right], \tag{29}$$

where $\alpha=1/3$, $t_0=-1800$ MeV fm^3, and $t_3=12871$ MeV fm$^{3(\alpha+1)}$. For these values of the interaction parameters, the nuclear matter equation of state, $E(\rho)/A$, has a minimum at $E/A=-15.99$ MeV, $\rho_0=0.157$ fm^{-3} with $K_{nm}=226$ MeV, where E/A, ρ_0, and K_{nm} are the binding energy per nucleon, matter saturation density, and incompressibility coefficient for symmetric nuclear matter, respectively. This choice of the two-body interaction enables us to use the continuum RPA method to carry out a fully self-consistent calculation for giant resonances. Following Ref. [24], one can write the mean field potential V_{mf} as

$$V_{mf}=\frac{3}{4}t_0\rho(r)+\frac{\alpha+2}{16}t_3\rho^{\alpha+1}(r), \tag{30}$$

and the particle-hole interaction V_{ph} contributing to the isoscalar channel is given by [17]

$$V_{ph}=\delta(\boldsymbol{r}_1-\boldsymbol{r}_2)\left[\frac{3}{4}t_0+\frac{(\alpha+1)(\alpha+2)}{16}t_3\rho^\alpha\right]. \tag{31}$$

To begin with, we consider our results for isoscalar giant monopole, dipole, and quadrupole resonances which are fully self-consistent and numerically accurate. Then, we shall analyze the influence of various numerical approximations on the centroid energies and transition densities for these resonances. Finally, we shall illustrate the possible effects of the violation of self-consistency on the properties of these isoscalar giant resonances (ISGR).

A. Self-consistent continuum RPA results

We now present our results of fully self-consistent HF-CRPA calculations for ^{80}Zr, using the Skyrme interaction of Eq. (29) with spin-orbit and Coulomb interactions switched off. It was pointed out in Ref. [18] that in order to have cancellations of the hole-hole transitions occurring in G_0 [Eq. (2)] and obtain numerically accurate results, it is important to employ the same mean field and the same integration algorithm for the bound states and the single-particle Green's

TABLE I. Hartree-Fock single-particle energies (in MeV) for the bound states in ^{80}Zr nucleus obtained for the interaction parameters $t_0=-1800$ MeV fm^3, $t_3=12871$ MeV fm^4, and $\alpha=1/3$ using the small mesh size $dr=0.04$ fm.

Orbits	$0s$	$0p$	$0d$	$1s$	$0f$	$1p$	$0g$	$1d$	$2s$
Energy	−45.50	−39.14	−31.02	−26.74	−21.42	−15.33	−10.59	−3.98	−2.62

TABLE II. Values for density radial moments $\langle r^2\rangle$ and $\langle r^4\rangle$ in units of fm^2 and fm^4, respectively, together with the EWSR associated with the scattering operator $r^n Y_{LM}$, in units of fm$^{(2n)}$ MeV, for different mesh size dr (in fm) used in the HF calculations.

			EWSR				
dr	$\langle r^2\rangle$	$\langle r^4\rangle$	rY_{10}	r^3Y_{10}	$(r^3-\eta r)Y_{10}$	r^2Y_{00}	r^2Y_{20}
0.04	14.705	282.147	391.04	404545	169661	7667	19167
0.08	14.702	282.008	391.04	404346	169553	7665	19163
0.24	14.676	280.653	391.04	402403	168441	7651	19129

function using a small mesh size in double precision calculations. In the following, we first present our results of highly accurate calculations obtained using $dr_{HF}=0.04$ fm and $dr_{RPA}=0.04$ fm, and with no smearing ($\Gamma=0$ MeV), which we use as a basis for comparison with other calculations. We note that in common implementations of HF-RPA, one usually adopts the values of $(dr_{HF},dr_{RPA})=(0.1\text{ fm},0.3\text{ fm})$ and a smearing parameter of $\Gamma/2\sim 1.0$ MeV. In the following, we use the notation $dr=(dr_{HF},dr_{RPA})$, with the values of dr_{HF} and dr_{RPA} given in units of femtometer.

To facilitate our discussions, we have displayed in Table I the HF single-particle energies for ^{80}Zr obtained by using $dr_{HF}=0.04$ fm. In Table II, we give the values for the density radial moments $\langle r^2\rangle$, $\langle r^4\rangle$, and EWSRs [Eq. (9)] for various multipoles evaluated for different values of mesh size used in the HF calculation. In Table III, we present the values of the energy weighted transition strengths (EWTS) for free and CRPA responses obtained using the operators f_3, f_1, and f_η with $dr=(0.04,0.04)$ and $\Gamma=0$ MeV. The quantities S_1^{EW}, S_3^{EW}, S_{13}^{EW}, and S_η^{EW} in Table III denote the EWTS for the corresponding strength functions S_1, S_3, S_{13}, and S_η, respectively, see Eq. (28). The transition strengths associated with narrow states were determined from the residues of Green's function, using its real part [see Eq. (8)]. For the free response, we get sharp peaks at the bound state single particle-hole transitions associated with $L=1$. These transitions can be easily identified from Table I as $0g\rightarrow 0f$ (10.83), $1d\rightarrow 1p$ (11.35), $2s\rightarrow 1p$ (12.70), $1d\rightarrow 0f$ (17.43), $1d\rightarrow 0p$ (35.16), and $2s\rightarrow 0p$ (36.52), with corresponding transition energies given in brackets in MeV. We checked that the values of the EWTS for these sharp transitions agree with the corresponding values obtained directly from the particle and hole wave functions.

For the CRPA response function, the sharp peaks occur below the particle threshold at 15.33 MeV. In addition to these sharp transitions, we have contributions from the continuum starting at the particle threshold. We obtained accurate values for the contributions from the continuum by integrating the energy weighted strength function using the small energy steps of $dE=0.01$ MeV. It is seen from Table

TABLE III. The energy weighted transition strengths (S^{EW}) of the free and fully self-consistent HF-CRPA response functions for ^{80}Zr (in fm^6 MeV) calculated using $dr_{HF}=dr_{RPA}=0.04$ fm, $N_{RPA}=300$ with no smearing width ($\Gamma=0$ MeV).

Energy	S_3^{EW}	$-2\,\eta S_{13}^{EW}$	$\eta^2 S_1^{EW}$	S_η^{EW}
		Free response		
10.832306	87689	−221289	139609	6009
11.352610	47160	−99851	52854	163
12.709777	24341	−37010	14068	1399
17.437181	48562	−64831	21638	5369
35.163326	17114	−7514	825	10425
36.520494	5034	−2123	224	3135
15.0–18.0	465	393	528	1386
18.0–100.0	172707	−36767	5009	140949
100.0–150.0	1256	−609	89	736
Total	404328	−469601	234844	169571
		CRPA response		
0.078606	234852	−469709	234857	0
11.434169	4480	5	−1	4484
12.965783	1984	7	0	1991
15.0–18.0	6087	45	0	6132
18.0–100.0	156848	−42	2	156808
100.0–150.0	258	−13	1	246
Total	404509	−469707	234859	169661

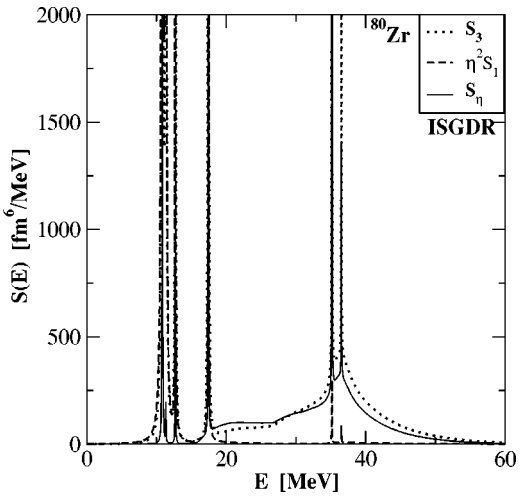

FIG. 1. Free response functions for the ISGDR calculated using the radial mesh size $dr=(0.04,0.04)$ with $\Gamma/2=0.025$ MeV and $\eta=24.51$ fm^2. The long dashed curve clearly manifests the existence of the spuriousity over the entire range of excitations but predominant for the $1\hbar\omega$ region ($E<18$ MeV).

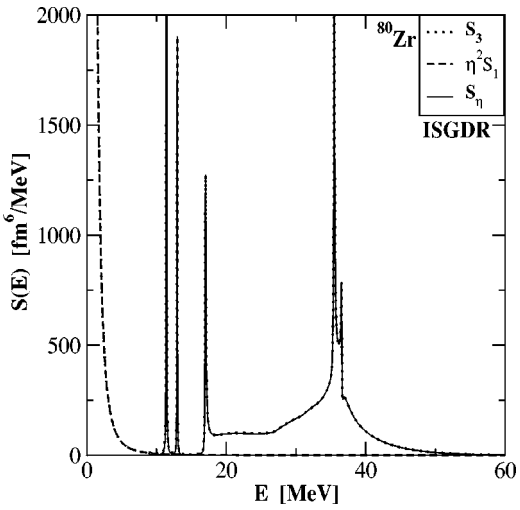

FIG. 2. Same as Fig. 1, but for the fully self-consistent HF-CRPA results. The response functions for the operators f_3 and f_η are almost the same indicating no spurious state mixing.

III that the spurious state mixing is significantly larger for the free response (see third column). Once the spurious state mixing is eliminated using the projection operator f_η, we find from the second and fifth columns of this table that most of the strengths of the free response in the $1\hbar\omega$ region of excitation energy ($E<18$ MeV) is spurious in nature. Only 6.8% of the EWTS for the operator f_3 contributes to the intrinsic excitations for $E<18$ MeV. On the other hand, in the case of CRPA, since the calculation is fully self-consistent and numerically very accurate, the resonance occurring at 0.079 MeV is fully spurious and it exhausts 99.99% of the EWSR associated with the operator f_1. For $E>0.08$ MeV, the values of S_1 and S_{13} are very small, with corresponding mixing probabilities of $b_n^2\sim10^{-8}$ [see Eq. (26)], indicating that the SSM is so small that one need not renormalize the strength S_η. Also, the values of the CRPA EWTS for the operators f_3 and f_η are the same within 1%. We would like to emphasize that though the spurious state mixing is significantly larger for the free response, it is fully eliminated by using the projection operator f_η giving rise to 99.95% of the expected EWSR which is quite close to the CRPA results. We note that the fraction energy weighted sum rule, FEWSR=EWTS/EWSR, for the operator f_η is 8.4% and 7.4% for $E<18$ MeV in the case of free and CRPA responses, respectively.

In Figs. 1 and 2, we have shown the free and the RPA response functions for the ISGDR, respectively, obtained from our most accurate calculations. For plotting purposes, we used a very small smearing width $\Gamma/2=0.025$ MeV. We see from Fig. 1 that most of the spurious components lie in the low energy region ($E<18$ MeV). As mentioned before, the response for the operators r^3 and $(r^3-\eta r)$ are indistinguishable in the case of a fully self-consistent HF based CRPA calculation. It also appears from these figures that particle-hole correlations do not alter the ISGDR strength distribution $S_\eta(E)$ very much suggesting that the isoscalar dipole state is not a very collective one.

An important test of a fully self-consistent calculation is to check how close $\rho_t(r,E_{ss})$ is to ρ_{ss}, where $\rho_t(r,E_{ss})$ is obtained from Eqs. (6) and (8) at the spurious state energy E_{ss} using f_1. In Fig. 3, we compare the CRPA result for the $\rho_t(r,E_{ss})$ with the coherent state transition density calculated using Eq. (16). It is seen in Fig. 3 that in this highly accurate HF-CRPA calculation, $\rho_t(r,E_{ss})$ coincides with ρ_{ss} indicating a very negligible SSM. We add further that at the surface, the transition density for the ISGMR resembles $3\rho_0+rd\rho_0/dr$ as given by Eq. (10), whereas, the ISGQR transition density resembles more $d\rho_0/dr$ rather than $rd\rho_0/dr$ as given by Eq. (10). We point out that Eq. (10) was derived under the assumption that one collective state exhausts the EWSR.

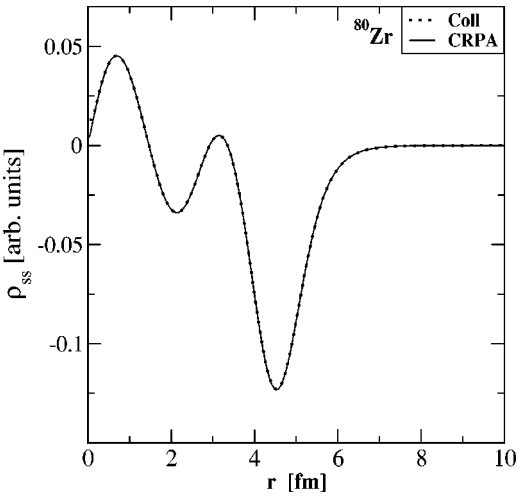

FIG. 3. Comparison of the fully self-consistent HF-CRPA result for the spurious state transition density obtained using the operator f_1 in Eq. (6) with the corresponding coherent spurious state transition density. The HF-CRPA calculation is carried out using the radial mesh size $dr=(0.04,0.04)$ with no smearing width ($\Gamma=0$ MeV).

TABLE IV. Fully self-consistent HF-CRPA results for the energy weighted transition strengths (in fm^6 MeV) for $\Gamma=0$ MeV using different mesh sizes (in fm) and $N_{RPA}=50$.

Energy	S_3^{EW}	$-2\eta S_{13}^{EW}$	$\eta^2 S_1^{EW}$	S_η^{EW}
		$dr_{RPA}=dr_{HF}=0.24$		
0.714539	232751	−465617	232866	0
11.483532	4214	−18	0	4196
13.138693	2306	−124	2	2184
15.0–18.0	5693	263	3	5959
18.0–100	154096	792	11	154899
100–150	184	−7	1	178
Total	399244	−464711	232883	167416
		$dr_{RPA}=6dr_{HF}=0.24$		
11.429694	4470	43	0	4513
12.962171	1998	−2	−4	1992
15.0–18.0	6158	−43	1	6116
18.0–100.0	159022	−2693	45	156374
100.0–150.0	363	−126	19	256
Total	172011	−2821	61	169251
		$dr_{RPA}=6dr_{HF}=0.24,\ V_{sc}=0.9916$[a]		
0.099965	237622	−474392	236771	1
11.430431	4505	−27	0	4478
12.959961	2025	−20	0	2005
15.0–18.0	6288	−157	3	6134
18.0–100.0	159324	−2992	52	156384
100.0–150.0	368	−128	19	259
Total	410132	−477716	236845	169260

[a]Normalization of the particle-hole interaction to put the spurious state at 0.1 MeV.

We have repeated the fully self-consistent calculations for $\Gamma=0$ MeV using various values of dr_{HF} and dr_{RPA}. In Table IV, we present CRPA results for the EWTS only for $dr=(0.24,0.24)$ and $(0.04,0.24)$ with $N_{RPA}=50$. We see from Table IV that the results for the operator f_3 for the different combinations of the mesh sizes differ by about 2.5%. The spurious state for $dr=(0.24,0.24)$ occurs at 0.7 MeV and its excitation energy becomes imaginary for $dr=(0.04,0.24)$. By multiplying the particle-hole interaction by a constant factor $V_{sc}=0.9916$, we push the spurious state to 0.1 MeV for $dr=(0.04,0.24)$ calculations. Nevertheless, we find that the SSM is very small ($b_n^2\sim 10^{-6}$). Once the spurious components are eliminated using the projection operator f_η, we get 99.40% and 99.76% of the expected EWSR for $dr=(0.24,0.24)$ and $(0.04,0.24)$, respectively.

In Tables V and VI, we have collected the centroid energies and the FEWSR, respectively, for the isoscalar giant resonances with $L=0$, 1, and 2 calculated using different combinations of the mesh size and a very small value of $\Gamma/2=0.025$ MeV. We notice that as long as the particle-hole interaction is not renormalized (i.e., $V_{sc}=1.0$), the centroid energies of the resonances do not deviate by more than 0.5% compared with the most accurate values. Though the energy of the spurious state is sensitive to the values of the mesh sizes and increases from 0.08 MeV to 0.71 MeV with an increase of radial mesh size from 0.04 fm to 0.24 fm, the centroid energy for the ISGDR changes only by about 0.08 MeV. Even if V_{sc} is used to shift the spurious peak to 2.0

TABLE V. HF based CRPA results for the spurious state energy E_{ss} and centroid energy E_L, for the ISGMR ($L=0$), ISGDR ($L=1$) and ISGQR ($L=2$) (in MeV), obtained using $\Gamma/2=0.025$ MeV. For the ISGMR and ISGQR we use the energy range 0–80 MeV and that for the ISGDR we use 28–80 MeV.

dr_{hf}	dr_{rpa}	V_{sc}	E_{ss}	E_0	E_1	E_2
0.04	0.04	1.0	0.08	22.98	35.88	14.67
0.08	0.08	1.0	0.18	22.97	35.86	14.70
0.24	0.24	1.0	0.71	22.92	35.80	14.69
0.04	0.24	1.0	a	22.94	35.83	14.60
0.04	0.24	0.9916	0.09	22.98	35.85	14.70
0.04	0.24	0.9707	2.00	23.08	35.88	14.96

[a]E_{ss} is imaginary.

TABLE VI. HF-CRPA results for fraction energy weighted sum rule (in percent) for the spurious state (SS) and the $L=0-2$ isoscalar giant resonances in the energy region 0–80 MeV, calculated using various radial mesh sizes dr_{HF} and dr_{RPA} (in fm) and $\Gamma/2=0.025$ MeV [for the spurious state we use $\Gamma=0$ and Eq. (8)]. See Table V for the corresponding values of E_{ss}.

dr_{HF}	dr_{RPA}	V_{scale}	SS	$L=0$	$L=1$	$L=2$
0.04	0.04	1.0	99.99	99.84	99.61	99.91
0.08	0.08	1.0	99.95	99.76	99.76	99.91
0.24	0.24	1.0	99.55	99.74	99.25	99.49
0.04	0.24	1.0	a	102.05	99.57	101.18
0.04	0.24	0.9916	101.22	102.02	99.57	101.17
0.04	0.24	0.9707	101.58	102.96	99.34	101.15

[a]The corresponding E_{ss} is imaginary.

MeV, the centroid energy for $L=0$ and $L=1$ resonances do not change appreciably. However, the centroid energy for the $L=2$ resonance goes up by about 2% (0.3 MeV). From Table VI, we find that when $dr=(0.04,0.24)$, the values of the total EWTS for ISGMR and ISGQR are overestimated by 1–2 %.

So far we have demonstrated that (i) as long as the calculation is fully self-consistent and numerically highly accurate, there is practically no spurious state mixing, and (ii) the spurious state mixing introduced due to the use of a large mesh size (0.24 fm) in a CRPA calculation can be projected out using the operator f_η.

B. Influence of the smearing parameter Γ

One of the requirements to avoid any SSM is that one must not use any smearing parameter (i.e., $\Gamma=0$) and the calculations should be performed using a very fine mesh in the coordinate space while solving HF and RPA equations. However, one typically uses $\Gamma/2\sim1.0$ MeV and the mesh $dr\geqslant0.1$ fm. If the smearing width is finite, the spurious state would have a long energy tail which can give rise to a large SSM. Since, $\rho_{ss}\propto d\rho_0/dr$, which is a surface peaked function and has a large matrix element for the operator f_3, one must project out the SSM by making use of the projection operator f_η.

In Fig. 4, we plot CRPA results for the spurious state and ISGDR strength functions calculated using a radial mesh size of 0.04 fm and a smearing parameter $\Gamma/2=1$ MeV. We clearly see from the figure that the strength function for the spurious state is extended up to a very high energy. The SSM caused due to the energy tail of the spurious state is eliminated using the operator f_η. In Table VII, we give the values of FEWSR associated with the scattering operator f_η for the ISGDR for various energy ranges up to 150 MeV obtained by using different values for the mesh size and the smearing parameter in the HF-CRPA calculation. Considering the values of the FEWSR in each energy range $\omega_1-\omega_2$ of Table VII, it can be easily seen that these values are practically the same as those obtained with $\Gamma=0$, i.e., the SSM due to nonzero Γ is completely projected out. In particular, for $\Gamma/2=1.0$ MeV, the values for FEWSR for the energy range $E=0-20$ MeV is lower by about 0.5% as compared to that for $\Gamma=0$. We also note that for $\Gamma/2=1.0$ MeV, the total FEWSR obtained by integrating up to $E=150$ MeV is about 1% lower than the one obtained for $\Gamma=0$. Of course, this is due to the remaining strength beyond 150 MeV. For instance, in the case of $dr=(0.24,0.24)$ and $\Gamma/2=1.0$ MeV, we get FEWSR=0.48% for the region for $E=150-300$ MeV.

We point out that due to $\Gamma\neq0$, the transition density ρ_t calculated using Eq. (6) depends on the scattering operator *f*. The consequences of this on the $S(E)$ and ρ_t of the ISGDR was investigated and discussed in detail in Ref. [9] and we will not repeat it here. We have thus demonstrated that using the projection scattering operator f_η, one can accurately eliminate the SSM effects on $S(E)$ and ρ_t of the ISGDR occurring due to the use of a finite smearing parameter $\Gamma/2$.

C. HF-DRPA results

We now consider our results obtained by discretizing the continuum using boxes of different sizes and different values of the particle-hole energy cutoff E_{ph}^{max} ranging from 50 to 600 MeV. The length of the box is given by N_{HF} times dr_{HF}, where N_{HF} is the number of radial mesh points used in a HF calculation. In the following, we present the results

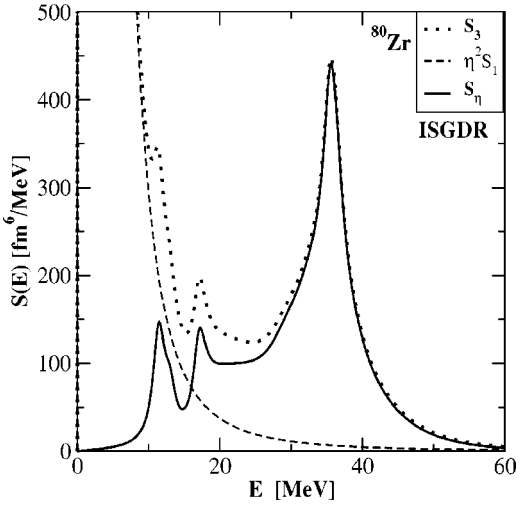

FIG. 4. Strength functions for the spurious state and ISGDR calculated using the radial mesh size $dr=(0.04,0.04)$ and the smearing parameter $\Gamma/2=1$ MeV in CRPA. The SSM caused due to the long tail of the spurious state is projected out using the operator f_η.

TABLE VII. CRPA results for the fraction energy weighted sum rule (in percent) of the ISGDR obtained using the operator f_η for the energy range $\omega_1-\omega_2$ (in MeV) for various combinations of the mesh size (in fm) and smearing parameter $\Gamma/2$ (in MeV).

			$\omega_1-\omega_2$				
dr_{HF}	dr_{RPA}	$\Gamma/2$	0–15	15–20	20–100	100–150	Total
0.04	0.04	0.0	3.82	5.73	90.30	0.15	100.00
0.04	0.04	0.025	3.81	5.71	90.28	0.16	99.96
0.04	0.04	0.25	3.79	5.66	90.05	0.27	99.77
0.04	0.04	1.0	3.69	5.37	89.39	0.65	99.10
0.24	0.24	0.0	3.79	5.57	89.93	0.11	99.40
0.24	0.24	1.0	3.63	5.15	89.12	0.61	98.51
0.04	0.24	0.0	3.83	5.72	90.05	0.15	99.75
0.04	0.24	1.0	3.71	5.25	89.26	0.65	98.87
0.08[a]	0.24	1.0	3.70	5.22	80.40	0.00	89.32
0.08[b]	0.24	1.0	3.83	5.46	88.45	0.00	97.74
0.08[c]	0.24	1.0	3.88	5.53	88.66	1.22	99.29

[a]HF-DRPA result with $E_{ph}^{max}=50$ MeV.
[b]HF-DRPA result with $E_{ph}^{max}=100$ MeV.
[c]HF-DRPA result with $E_{ph}^{max}=200$ MeV.

for discretized RPA calculations obtained by using $dr=(0.08,0.24)$ with $N_{HF}=150$ and 900 (box sizes of 12 and 72 fm, respectively).

To examine more closely the effects of cutoff energy E_{ph}^{max} on the response function, we present in the last three rows of Table VII our DRPA results for the FEWSR over various energy ranges up to 150 MeV obtained using $E_{ph}^{max}=50$, 100, and 200 MeV. Comparing the values of the FEWSR, in each of the energy range $\omega_1-\omega_2$, of Table VII (particularly the energy ranges of 0–15 and 15–20 MeV), we conclude that by using f_η, one accurately eliminates SSM occurring due to the use of a low value for E_{ph}^{max}. This is also demonstrated in Fig. 5.

It is evident from Table VII that the total FEWSR increases significantly when E_{ph}^{max} is increased from 50 MeV to 200 MeV. This increase is about 9–10 % for $\Gamma/2=1$ MeV. With a further increase in E_{ph}^{max}, there is no noticeable change in the value of the total FEWSR. In Fig. 6, we show the ISGDR response functions obtained by using the box sizes of 12 and 72 fm, a smearing parameter $\Gamma/2=1.0$ MeV and $E_{ph}^{max}=200$ MeV, together with the corresponding results obtained in HF-CRPA. We see that the DRPA results obtained for the larger box coincide with the results obtained within CRPA. The transition strength gets fragmented if the discretization is carried out using a small box. To avoid a misleading interpretation of the fragmentation and obtain agreement with the CRPA results, one needs to use a larger value of the smearing parameter consistent with the size of the box. Therefore, one can satisfactorily reproduce the CRPA results, provided the DRPA calculations are carried out using a box of very large size (i.e., dense discretization) and the cutoff for the particle-hole excitation energy (E_{ph}^{max}) is set to be reasonably high.

We have demonstrated in Fig. 3 that the spurious transition density $\rho_t(r,E_{ss})$ obtained by using a fully self-consistent CRPA calculation is indistinguishable from the corresponding collective model form for ρ_{ss} which is proportional to $d\rho_0/dr$. In Fig. 7, we show some of the DRPA results for $\rho_t(r,E_{ss})$ and compare them with the ρ_{ss}. We see that for $E_{ph}^{max}=50$ MeV, $\rho_t(r,E_{ss})$ deviates from $d\rho_0/dr$. However, for $E_{ph}^{max}=200$ MeV, the $\rho_t(r,E_{ss})$ from the DRPA is almost identical to the collective model results. We thus conclude that one must use a reasonably large value for the cutoff energy E_{ph}^{max} in order to fully eliminate from the intrinsic excitations the contribution due to SSM.

In Table VIII, we have displayed the values of E_{ss} and the centroid energies for the $L=0$, 1, and 2 isoscalar giant resonances. These results are obtained by using $N_{HF}=900$ and $\Gamma/2=0.25$ MeV with different values of E_{ph}^{max} in the HF-

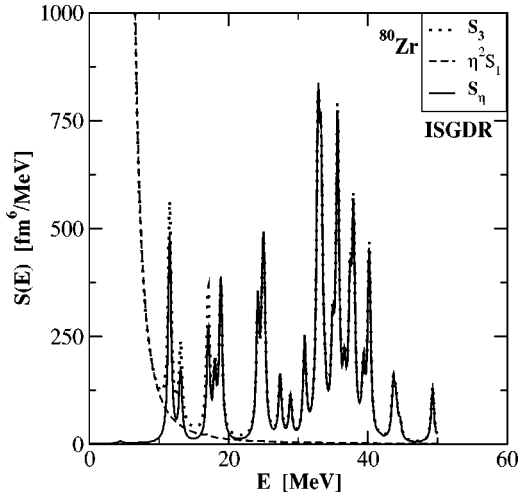

FIG. 5. Discretized RPA results of strength functions for the spurious state and the ISGDR obtained using $N_{HF}=150$ with $dr=(0.08,0.24)$ and a smearing parameter $\Gamma/2=0.25$ MeV. We use a particle-hole cutoff energy $E_{ph}^{max}=50$ MeV. The SSM caused due to the low cutoff energy and the tail of the spurious state is projected out using the operator f_η.

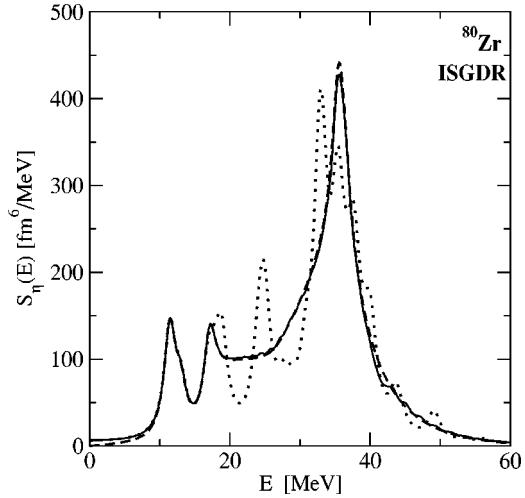

FIG. 6. Discretized RPA results for the ISGDR response functions obtained using the smearing parameter $\Gamma/2=1.0$ MeV. The discretization is performed using $N_{HF}=150$ (dotted line) and $N_{HF}=900$ (solid line) with $dr=(0.08,0.24)$. We use particle-hole cutoff energy $E_{ph}^{max}=200$ MeV. The corresponding HF-CRPA result is shown by a long dashed curve.

DRPA calculations. The corresponding HF-CRPA results are given in the last row of the table. We clearly see that as E_{ph}^{max} increases, the centroid energies E_0, E_1, and E_2 converge to their corresponding exact values obtained using HF-CRPA. However, this convergence is slower for the spurious state energy E_{ss}. For low values of E_{ph}^{max}, we observe that the centroid energy for ISGMR is overestimated by about 0.5 MeV, which can significantly affect the value determined for the nuclear incompressibility.

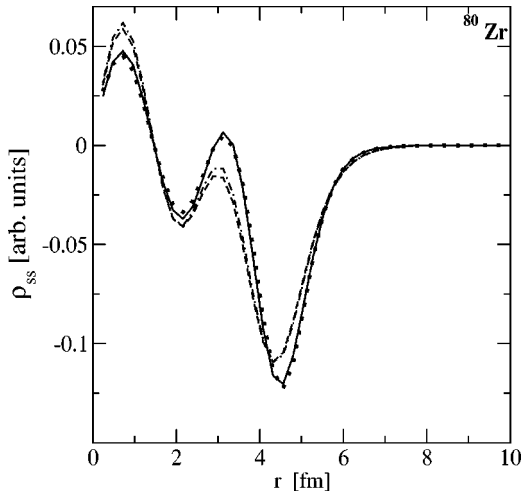

FIG. 7. Similar to Fig. 3 but for the HF-DRPA results. The dash-dot, long dash, and solid curves represent the DRPA results for N_{HF} $(E_{ph}^{max})=150$ (50 MeV), 900 (50 MeV), and 900 (200 MeV), respectively. The transition density do not change significantly when N_{HF} increases from 150 to 900, but, with increase in E_{ph}^{max} the DRPA results become closer to the coherent spurious state transition density [Eq. (10)].

TABLE VIII. Dependence of E_{ss} and the centroid energies E_L ($L=0$, 1, and 2), in MeV, on the value of E_{ph}^{max} (in MeV) used in the HF-DRPA calculations. We have used the values of $N_{HF}=900$, $N_{RPA}=50$, $dr=(0.08,0.24)$, and $\Gamma/2=0.25$ MeV. The corresponding HF-CRPA results are given in the last row.

E_{ph}^{max}	E_{ss}	E_0	E_1	E_2
50	4.7	23.92	35.34	16.11
75	3.3	23.51	35.76	15.51
100	2.9	23.25	35.66	15.14
200	1.5	23.09	35.55	14.82
400	1.0	23.02	35.51	14.73
600	0.9	23.02	35.51	14.72
∞	0.7	23.01	35.46	14.70

D. Effects of violation of self-consistency

So far, we have examined the various effects of numerical approximation on the properties of the isoscalar giant resonances of multipolarity $L=0-2$ and established the validity of the projection operator method in eliminating the SSM effects from the $S(E)$ and $\rho_t(r)$ of the ISGDR. Here we report on our investigations of the influence of certain violations of self-consistency on the strength function for isoscalar giant monopole ($L=0$), dipole ($L=1$), and quadrupole ($L=2$) resonances. These investigations are quite important in view of the fact that one often performs non-self-consistent calculations for giant resonances, such as the use of a phenomenological nuclear mean field (e.g., Woods-Saxon potential) and a Landau-Migdal particle-hole interaction [8]. Moreover, one often comes across HF-RPA calculations carried out using particle-hole interaction not consistent with the mean field used in HF. We present below the results for HF based CRPA calculations carried out with the two-body interaction given in Eq. (29). We use the parameter V_{sc} to renormalize the particle-hole interaction [i.e., $t_0 \rightarrow t_0 V_{sc}$ and $t_3 \rightarrow t_3 V_{sc}$ in Eq. (31)] so that the position of the spurious state can be adjusted close to zero. To study the consequences of the violation of self-consistency, we vary t_0 and t_3 only in the particle-hole interaction [only in Eq. (31)].

In Table IX, we summarize our results for the centroid energies of isoscalar giant resonances of multipolarity $L=0-2$. The quantity K'_{nm} is the nuclear matter incompressibility coefficient associated with the renormalized parameters $t_0 V_{sc}$ and $t_3 V_{sc}$ employed in the particle-hole interaction. Let us first consider the results obtained by varying t_0 by $\pm 5\%$ and $\pm 10\%$ and keeping $t_3=12871$ MeV fm^4. It can be clearly seen from the table that the centroid energies for ISGMR and ISGDR significantly differ from their corresponding self-consistent values even if V_{sc} is adjusted to give the $E_{ss}=0.1$ MeV. On the other hand, the centroid energy for the ISGQR reattains its self-consistent value when V_{sc} is adjusted to yield $E_{ss}=0.1$ MeV. One may understand this discrepancy in terms of the incompressibility coefficient. With the renormalization of V_{ph}, though, the E_{ss} becomes close to zero, but the values of K'_{nm} in the RPA calculation remain quite different than the HF value of 226 MeV. In Fig. 8, we plot the values of E_0 and E_1 versus $\sqrt{K'_{nm}}$ for the cases

TABLE IX. HF-CRPA results for the spurious state energy E_{ss}, incompressibility coefficient K'_{nm}, and centroid energy E_L (in MeV) for isoscalar giant resonances for $L=0-2$ with different values of t_0, t_3, and V_{sc} used in the particle-hole interaction. These calculations are performed using $\Gamma/2=0.25$ MeV and $dr_{HF}=dr_{RPA}=0.04$ fm.

t_0	t_3	V_{sc}	K'_{nm}	E_{ss}	E_0	E_1	E_2
−1800	12871	1.0	226	0.1	23.1	35.5	14.8
−1710	12871	1.0	258	6.7	26.3	37.9	17.4
−1710	12871	1.2938	321	0.1	26.0	38.2	14.7
−1620	12871	1.0	289	9.2	29.0	40.0	19.5
−1620	12871	1.7118	464	0.1	29.8	41.8	14.7
−1620	11875	1.0	226	5.9	24.9	36.7	16.8
−1620	11875	1.2264	267	0.1	24.4	36.8	14.8
−1620	11270	1.0	188	0.1	21.6	34.4	14.8
−1890	12871	1.0	194	a	18.7	32.8	11.1
−1890	12871	0.7910	163	0.1	20.8	33.7	14.8
−1980	12871	1.0	162	a	11.4	29.9	2.1
−1980	12871	0.6398	120	0.1	19.2	32.6	14.9
−1980	13875	1.0	226	a	20.8	34.2	12.1
−1980	13875	0.8408	197	0.1	22.1	34.7	14.8
−1980	14500	1.0	266	0.1	24.3	36.6	14.7

[a] E_{ss} is imaginary.

with $E_{ss}=0.1$ MeV. This plot clearly depicts the systematic increase of E_0 and E_1 with the increase of K'_{nm}. One may be tempted to infer at this point that as long as the nuclear matter incompressibility associated with the particle-hole interaction and the mean field is the same, centroid energies for the resonances considered here may be reliable. In order to verify this, we adjust t_3 in the particle-hole interaction in such a way that K'_{nm} becomes 226 MeV when t_0 is varied by $\pm 10\%$. We see from Table IX that even if K'_{nm} is adjusted to

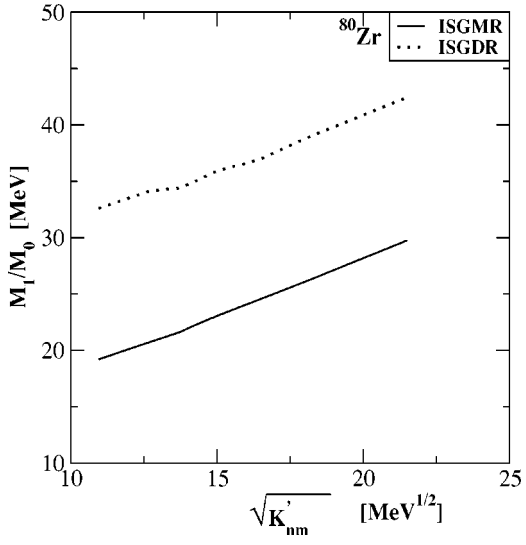

FIG. 8. The centroid energies E_0 and E_1 versus $\sqrt{K'_{nm}}$ for ^{80}Zr. Here, K'_{nm} denotes the nuclear matter incompressibility coefficient associated with the parameters used in particle-hole interaction (see also the text).

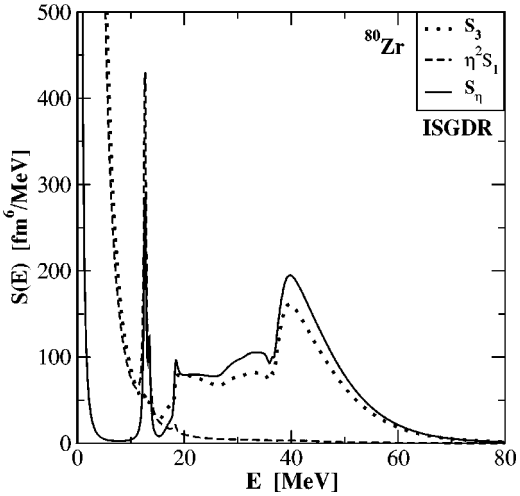

FIG. 9. Non-self-consistent CRPA results for the spurious state and the ISGDR strength functions associated with the operators f_1, f_3, and f_η calculated by using $t_0=-1620$ MeV fm^3, radial mesh size $dr=(0.04,0.04)$, and $\Gamma/2=0.25$ MeV. The strength function for the operator f_η is larger than that for the operator f_3 for a wide range of energy.

226 MeV, the values of E_0 and E_1 are off by about 10% and 3.5%, respectively. This is due to the fact that the shape of the particle-hole interaction is not the same, though K'_{nm} is kept constant. We note that if the ISGMR centroid energy is determined within 10% accuracy, the value of nuclear matter incompressibility coefficient will be correct only within 20%.

Apart from the centroid energies for the giant resonances, it is also important to investigate the effects on the strength function itself when self-consistency is not maintained. We observed the plots for the ISGDR strength functions S and S_η associated with the operators f_3 and f_η, respectively, for the different cases listed in Table IX. We find either $S_3 \geqslant S_\eta$ or $S_3 < S_\eta$ depending on the sign of interference between the spurious state and the intrinsic state (i.e., sign of the non-diagonal strength S_{13}). As an illustrative example, we show in Fig. 9 our results for the case in which t_0 is varied by -10% and $V_{sc}=1.7118$. The case is similar when t_0 is varied by -5% and $V_{sc}=1.2938$. These values of V_{sc} were chosen so that $E_{ss}=0.1$ MeV.

In Figs. 10(a)–(c), we compare the fully self-consistent results for isoscalar giant resonances with those obtained by varying t_0 by $\pm 5\%$ in Eq. (31) and V_{sc} is adjusted to yield $E_{ss}=0.1$ MeV. We see that the strength function for the ISGMR and the ISGDR are significantly different compared with their corresponding self-consistent results; whereas, in the case of the ISGQR, not only the centroid energies but also the strength function seem to agree well with the corresponding self-consistent results. Note that ρ_t of the ISGQR is very similar to ρ_{ss} (of the spurious state). It is very important to point out that the violation of self-consistency causes redistribution of the strength in such a way that the total EWTS remains unaltered. This redistribution may be crucial in determining the energy weighted strengths associated with the low energy and the high-lying energy components of the ISGDR. For example, the fraction of the EWSR (in percent)

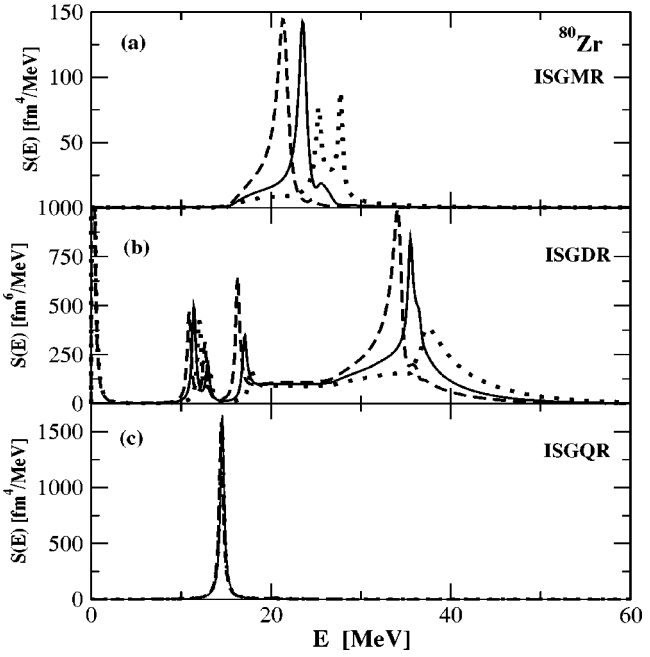

FIG. 10. Influence of violation of self-consistency due to variation of t_0 by $+5\%$ (dashed line) and -5% (dotted line) on the strength function for the (a) ISGMR, (b) ISGDR, and (c) ISGQR. The solid line represents the self-consistent result (i.e., $t_0 = -1800$ MeV fm^3).

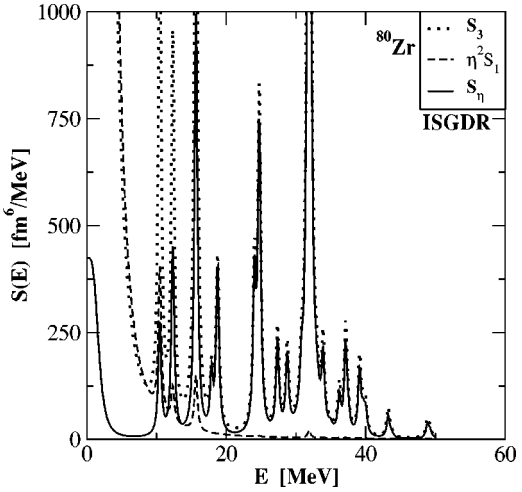

FIG. 11. DRPA results for the spurious state and the ISGDR strength functions obtained for $t_0 = -1980$ MeV fm^3 and $E_{ph}^{max} = 50$. The calculations were performed using, $N_{HF} = 150$, $dr = (0.08, 0.24)$, and $\Gamma/2 = 0.25$ MeV.

for the energy range $E = 0-20$ MeV is 6.94, 9.33, and 12.42 for $t_0 = -1710$, -1800, and -1890 MeV fm^3, respectively, and for $E = 0-150$ MeV, we have the FEWSR $= 99.76\%$ in all these three cases.

We now focus on the influence of self-consistency violation when the continuum is discretized. As seen above, the discretization introduces two additional constraints, namely, the box size used in the HF calculations and the maximum allowed particle-hole energy E_{ph}^{max}. We present here only the results for a box size of 12 fm with $E_{ph}^{max} = 50$ and 200 MeV. In Fig. 11, we show the ISGDR response functions obtained for $t_0 = -1980$ MeV fm^3, keeping $E_{ph}^{max} = 50$ MeV. When compared with the results of Fig. 5, one sees a marked enhancement in spuriousity at $E = 10-12$ MeV for the case with $t_0 \neq -1800$ MeV fm^3. Furthermore, it is interesting to see that the total FEWSR associated with the operator f_η for $t_0 = -1980$ MeV fm^3 is only 58.97% compared with 95.13% for $t_0 = -1800$ MeV fm^3. We repeated the same analysis for a box size of 72 fm keeping $E_{ph}^{max} = 50$ MeV but did not find any appreciable change in the values of the total FEWSR. When we raised the E_{ph}^{max} from 50 to 200 MeV, we got for the total FEWSR 99.94% and 100.52% for $t_0 = -1980$ and -1800 MeV fm^3, respectively. However, the large spuriousity at $E = 10-12$ MeV for the case with $t_0 \neq -1800$ MeV fm^3 persists. Similar results were obtained for other values of t_0.

We also calculate the SSM probabilities (i.e., b_n^2) when self-consistency is not maintained. The values of b_n^2 are extracted using an extremely small smearing parameter. In the case of $t_0 = -1620$ MeV fm^3 and $E_{ph}^{max} = 50$ MeV used in the DRPA calculation, we find that $E_{ss} = 9.84$ MeV. We get from Eq. (26), $b_n^2 = 2.4\%$ for the state occurring at ~ 13 MeV. When V_{sc} is adjusted to push the spurious state energy E_{ss} to about 0.1 MeV, the EWTS of the 13 MeV state associated with the f_1 operator remains unchanged. Consequently, b_n^2 is reduced by two orders of magnitude. We thus conclude that since the values of b_n^2 are less than a few percent even with a large violation of self-consistency, the renormalization of the strength function $S_\eta(E)$ may be ignored.

We have considered the effects on the ISGDR strength function when the Coulomb/spin-orbit interaction is switched on in the HF calculation, but ignoring it in the particle-hole interaction. We find that when the spin-orbit interaction is included, the strength function obtained using $\Gamma/2 = 1.0$ MeV is hardly affected at any energy and the differences cannot be seen on the plots (not shown here). This is due to the fact that the nucleus in question, ^{80}Zr, is spin saturated, i.e., the single-particle states with $j = l \pm 1/2$ are occupied. However, this may not be the case for non-spin-saturated heavy nuclei. When we carried out a similar exercise with the Coulomb interaction, the mean field changed significantly and we found that the strength functions get shifted toward lower energy by about 2.0 MeV. We note that with the inclusion of Coulomb interaction, the particle threshold energy for protons reduces from 15.33 MeV to 3.5 MeV.

IV. CONCLUSIONS

We have carried out self-consistent HF based CRPA calculations for isoscalar giant resonances with multipolarities $L = 0$, 1, and 2 for the ^{80}Zr nucleus as an example. We demonstrated that if a self-consistent calculation is performed using zero smearing width and a very fine radial mesh size ($dr = 0.04$ fm), the spurious state occurs at the $E_{ss} = 0.08$ MeV and the ISGDR response functions for the operators f_3 and f_η are essentially the same for energy E

$>E_{ss}$, which indicates no SSM. The corresponding EWSR is reproduced remarkably well. When we use $dr=0.24$ fm in HF and CRPA calculations, the E_{ss} becomes ≈ 0.7 MeV and there exists a small SSM. The amplitude of this SSM (i.e., b_n^2) $\sim 10^{-6}$, which is negligible and one need not renormalize the projected strength function. Although the position of the spurious state is quite sensitive to the radial mesh size and smearing parameter Γ, the centroid energy for the isoscalar resonances for $L=0$, 1, and 2 do not change by more than 0.5%.

We have also performed the calculation for $L=0$, 1, and 2 isoscalar giant resonances by discretizing the continuum using boxes of different sizes (12 and 72 fm) with E_{ph}^{max} ranging from 50–600 MeV. For the case of discretization in a large box (72 fm) with $E_{ph}^{max}=200$ MeV, we find that the strength distribution agrees reasonably well with the corresponding one obtained from CRPA if a moderate value of the smearing parameter ($\Gamma/2\sim 1.0$ MeV) is used. The spurious state occurs at about 4.5 MeV for $E_{ph}^{max}=50$ MeV for both the small as well as the large box discretization considered. With the increase of E_{ph}^{max} to 600 MeV, we find that the E_{ss} approaches the corresponding value obtained within the CRPA. Further, the centroid energies for $L=0$, 1, and 2 resonances converge to their corresponding exact values obtained from HF-CRPA. This convergence is somewhat slower in the case of the spurious state energy. For $E_{ph}^{max}=50$ MeV, the transition density $\rho_t(r,E_{ss})$ at the spurious state energy obtained using discretized RPA differs from the corresponding CRPA results (which reproduce ρ_{ss}). However, with an increase of E_{ph}^{max} to 200 MeV, the DRPA results for $\rho_t(r,E_{ss})$ become quite close to the CRPA results. We also point out that one should use $E_{ph}^{max}\geqslant 200$ MeV in order to calculate the centroid energies of the isoscalar $L=0$, 1, and 2 resonances with the accuracy of 0.1 MeV, comparable to the current experimental uncertainties.

We have demonstrated that the spurious state mixing due to the nonzero smearing width and a choice of a coarse sized radial mesh can be accurately eliminated using the projection operator f_η. Furthermore, we show that the SSM due to a small value of E_{ph}^{max} used in the DRPA calculation can be fully eliminated by applying the projection method.

We have investigated the consequences of violation of self-consistency on the $S(E)$ and ρ_t of the $L=0$, 1, and 2 isoscalar giant resonances by varying the parameter t_0 by $\pm 5\%$ and $\pm 10\%$ in the particle-hole interaction. We find that if the self-consistency is not maintained, then the values of the E_{ss} and centroid energies for the $L=0$, 1, and 2 isoscalar giant resonances are significantly different compared with their self-consistent values. Even if the particle-hole interaction is renormalized to shift the E_{ss} close to its self-consistent value, the centroid energies for the ISGMR and ISGDR deviate from the corresponding self-consistent values. This is due to the fact that though the renormalization corrects the value of the E_{ss}, the nuclear matter incompressibility coefficient K'_{nm} associated with the particle-hole interaction is quite different from the one associated with the interaction used in the mean field. However, the $L=2$ resonance is not very sensitive to the self-consistency violation as long as the particle-hole interaction is renormalized to shift the E_{ss} close to its self-consistent value. It is also important to point out that the violation of self-consistency causes a significant redistribution of the transition strength. In particular, the energy weighted transition strength of the lower energy component ($E<20$ MeV) of the ISGDR response function may differ by 50%. The values of the SSM probabilities b_n^2 were found to be less than 1–2 %. Therefore, one can neglect the renormalization of the ISGDR strength function obtained using the projection operator f_η. Further, we found that the total energy weighted transition strength for the operator f_η remains unaltered even with the violation of self-consistency.

Calculations were also carried out by changing the parameters appearing in the particle-hole interaction in such a way that the nuclear matter incompressibility coefficient associated with it remains unaltered. We find that though the incompressibility coefficient associated with the particle-hole and the mean field are kept the same; due to the lack of self-consistency, the centroid energies of the $L=0$ and 1 isoscalar giant resonances are off by 10% and 3.5%, respectively, compared to their self-consistent values. We may remark that if the ISGMR centroid energy is determined within an accuracy of 10%, the value of K_{nm} deduced from a comparison with experimental data is then accurate only within 20%.

ACKNOWLEDGMENTS

This work was supported in part by the U.S. Department of Energy under Grant No. DOE-FG03-93ER40773.

[1] A. Bohr and B. Mottelson, *Nuclear Structure* (Benjamin, London, 1975), Vol. II, Chap. 6.
[2] S. Stringari, Phys. Lett. **108B**, 232 (1982).
[3] S. Shlomo and D.H. Youngblood, Phys. Rev. C **47**, 529 (1993), and references therein.
[4] J.P. Blaizot, Phys. Rep. **64**, 171 (1980).
[5] H.L. Clark, Y.-W. Lui, and D.H. Youngblood, Phys. Rev. C **63**, 031301(R) (2001), and references therein.
[6] I. Hamamoto, H. Sagawa, and X.Z. Zhang, Phys. Rev. C **57**, R1064 (1998).
[7] A. Kolomiets, O. Pochivalov, and S. Shlomo, *Progress in Research* (Cyclotron Institute, Texas A&M University, Texas, 1999), p. III-1.
[8] M.L. Gorelik, S. Shlomo, and M.H. Urin, Phys. Rev. C **62**, 044301 (2000).
[9] S. Shlomo and A.I. Sanzhur, Phys. Rev. C **65**, 044310 (2002); S. Shlomo, Pramana, J. Phys. **57**, 557 (2001).
[10] G. Colo, N. Van Giai, P.F. Bortignon, and M.R. Quaglia, Phys. Lett. B **485**, 362 (2000).
[11] D. Vretenar, A. Wandelt, and P. Ring, Phys. Lett. B **487**, 334 (2000).
[12] J. Piekarewicz, Phys. Rev. C **62**, 051304(R) (2000).

[13] T.S. Dumitrescu and F.E. Serr, Phys. Rev. C **27**, 811 (1983).
[14] H.P. Morsch, M. Rogge, P. Turek, and C. Mayer-Boricke, Phys. Rev. Lett. **45**, 337 (1980).
[15] C. Djalali, N. Marty, M. Morlet, and A. Willis, Nucl. Phys. **A380**, 42 (1982).
[16] B. Davis *et al.*, Phys. Rev. Lett. **79**, 609 (1997).
[17] G.F. Bertsch and S.F. Tsai, Phys. Rep. **18**, 125 (1975).
[18] S. Shlomo and G.F. Bertsch, Nucl. Phys. **A243**, 507 (1975).
[19] B. K. Agrawal and S. Shlomo, *Progress in Research* (Cyclotron Institute, Texas A&M University, Texas, 2002), pp. III-19, III-21, and III-22.
[20] I. Hamamoto and H. Sagawa, Phys. Rev. C **66**, 044315 (2002).
[21] J.V. Noble, Ann. Phys. (N.Y.) **67**, 98 (1971).
[22] T.J. Deal and S. Fallieros, Phys. Rev. C **7**, 1709 (1973).
[23] G.F. Bertsch, Suppl. Prog. Theor. Phys. **74**, 115 (1983).
[24] D. Vautherin and D.M. Brink, Phys. Rev. C **5**, 626 (1975).